# Prediction of DNB in the tube and annulus channel at high pressure using Eulerian-Eulerian two-phase flow model in STAR-CCM+

Tae Young Yang, Giwon Bae, Hyoung Kyu Cho\* Department of nuclear engineering, Seoul National Univ., 1 Gwanak-ro, Gwanak-gu, Seoul 08826 \*Corresponding author: chohk@snu.ac.kr

## \*Keywords: DNB, Multiphase CFD, Star-CCM+, Annulus geometry, Tube geometry

#### 1. Introduction

Subcooled flow boiling has been widely used in many industrial fields due to its high heat transfer efficiency. However, excessive boiling can lead to local vapor dryspots on the heated surface. The corresponding heat flux is called critical heat flux (CHF). At CHF, the temperature of the heater can rise rapidly and lead to damage of the heating surface. Therefore, accurate prediction of the critical heat flux (CHF) is important in the nuclear energy industry for reactor safety.

recent advancements in computational capabilities, there has been a growing interest in developing CHF prediction models using multiphase CFD methodology. It is believed to be a more costsaving approach than the conventional high-budget, time-consuming experiments, and can provide much more detailed information than the lumped subchannel analysis [1].

Recently, under the CASL (Consortium for Advanced Simulation of Light Water Reactors) program, a CHF prediction model known as the CASL FY19 model was developed using STAR-CCM+. However, according to performance evaluation reports [2], the CASL FY19 model tends to underestimate CHF. The findings point to possible improvements achievable through model modifications. Furthermore, validation of the model has been limited to tube and fuel assembly geometries, leaving its predictive performance for annular geometries uncertain. Therefore, in this study, several physical models were modified to improve upon the CASL FY19 model, and their predictive performance was compared and analyzed.

### 2. Numerical method

This section provides the conservation equations and boiling models used in this calculation and describes the differences between the CASL FY19 models and the present model of the present work. Detail description of test section, calculated experiment conditions, and calculation methodology are also provided

# 2.1. STAR-CCM+ Eulerian multiphase approach

In this study, the STAR-CCM+ software was used. S TAR-CCM+ provides the Eulerian multiphase (EMP) framework known to be highly effective in simulating subcooled boiling. This framework solves governing equations of mass, momentum, and energy conservation for each phase. The Eulerian–Eulerian approach solves conservation equations for each phase with assumptions that all phases coexist within each computational cell, with the sum of their volume fractions equal to unity. Interfacial mass, momentum, and energy exchange are described through several closures and reflected in the conservation equations. The conservation equations for mass, momentum, and energy in two-fluid models can be expressed in the Equations (1)  $\sim$  (3).

Mass

$$\frac{\partial(\alpha_k \rho_k)}{\partial t} + \nabla \cdot (\alpha_k \rho_k \mathbf{u_k}) = \Gamma_k \tag{1}$$

Momentum
$$\frac{\partial(\alpha_k \rho_k)}{\partial t} + \nabla \cdot (\alpha_k \rho_k \mathbf{u}_k) = \Gamma_k \tag{1}$$

$$\frac{\partial(\alpha_k \rho_k \mathbf{u}_k)}{\partial t} + \nabla \cdot (\alpha_k \rho_k \mathbf{u}_k \mathbf{u}_k)$$

$$= -\nabla(\alpha_k p_k) + \nabla \cdot (\alpha_k \tau_k) + \alpha_k \rho_k \mathbf{g} + \mathbf{M}_k^i \tag{2}$$
Energy

Energy
$$\frac{\partial(\alpha_{k}\rho_{k}e_{k})}{\partial t} + \nabla \cdot (\alpha_{k}\rho_{k}\mathbf{u}_{k}e_{k}) = -\nabla(\alpha_{k}q_{k}) + \nabla \cdot [\alpha_{k}(-p_{k}+\tau_{k})\cdot\mathbf{u}_{k}] + \alpha_{k}\rho_{k}\mathbf{g}\cdot\mathbf{u}_{k} + E_{k}^{i} \qquad (3)$$

where  $\alpha_k, \rho_k, \boldsymbol{u_k}$ , and  $e_k$  are the volume fraction, density, velocity, and specific internal energy.  $\Gamma_k$  is the net mass transfer rate,  $M_k^i$  represents the interfacial momentum forces, and  $E_k^i$  is the interfacial heat transfer

To model wall heat transfer, the computational framework in this study adopts the heat partitioning model of Kurul and Podowski [3]. The models are as follows.

Total heat flux

$$q'_{tot} = (1 - f(\alpha))(q'_{c,l} + q'_{q} + q'_{e}) + f(\alpha)q'_{c,v}$$
 (4)

$$q'_{tot} = (1 - f(\alpha))(q'_{c,l} + q'_q + q'_e) + f(\alpha)q'_{c,v}$$
(4)  
Liquid convection
$$q'_{c,l} = \frac{\rho_l c_{pl} u_l^*}{t_l^+} (T_w - T_l)$$
(5)

Quenching heat flux

$$q_q' = 2K_q f \sqrt{\frac{\rho_l c_{pl} k_l t_w}{\pi}} (T_w - T_l) \tag{6}$$

Evaporation heat flux 
$$q'_{e} = N' f \frac{\pi D_{d}^{3}}{6} \rho_{g} h_{v}$$
 (7) Vapor convection 
$$q'_{v} = \frac{\rho_{v} c_{pv} u_{v}^{*}}{t^{+}} (T_{w} - T_{l})$$
 (8)

$$q_{v}' = \frac{\rho_{v} c_{pv} u_{v}^{*}}{t_{l}^{+}} (T_{w} - T_{l})$$
 (8)

Here,  $f(\alpha)$  represents the vapor contact area fraction, which denotes the fraction of the surface area where single-phase heat transfer occurs through vapor. In the model of Weisman and Pei [4], that local wall dryout occurs when the void fraction in the bubbly layer exceeds a critical value.

## 2.2. Comparison of physics model

Each mass, momentum, and energy conservation equations include terms representing interfacial interactions, and the selection of appropriate models for these terms can significantly influence the simulation results. Accordingly, users select models that accurately capture the underlying physics of the system under investigation. The physics models employed in the CASL FY19 model and present model are described in Table I.

Table I. Physics model

	Table 1. Th	ysics model	
	Parameters	CASL FY19 [5]	Present model
Turbulence model	Turbulence	Standard k-epsilon linear	Standard k- epsilon linear
Interaction length scale	Interaction length scale	Modified S-gamma (Partially mobile interface)	Modified S- gamma (Fully mobile interface)
	Interaction area density	Symmetric	Symmetric
Interfacial momentum transfer	Drag coefficient	Tomiyama (Moderate contaminat e)	Tomiyama (Clean)
	Drag correction	Volume fraction exponent (0.0)	Simonnet correction
	Lift coefficient	Sugrue	Sugrue
	Wall lubrication force	Lubchenko	Lubchenko
Wall boiling	Departure diameter	Kocamusta -faogullari	Kocamusta- faogullari
	Departure frequency	Cole	Cole
	Nucleation site density	Li et al.	Li et al.
	Bubble influence area	Del Valle kenning (0.8)	Del Valle kenning (0.8)
	DNB detection	Analytical wall dryout	$\alpha_v > 0.9$ $y^+ = 200$
Interfacial heat transfer	Condensatio n fluid	Kim-Park	Ranz- Marshall
	Condensatio n vapor	$Nu_v = 26$	$Nu_v = 26$

Tomiyama [6] proposed three types of drag coefficient correlations: clean, moderate, and contaminated. Since all experimental data used in this study were obtained using clean water, the drag coefficient model was revised to the Tomiyama clean model.

As the Tomiyama drag coefficient model was originally developed for single bubbles, the Simonnet correction model was additionally applied to improve accuracy in the high void fraction region.

Furthermore, the fully mobile interface model was selected, as it provides an appropriate coalescence rate for pure working fluids. For condensation heat transfer, the Ranz–Marshall condensation model was used since it is widely utilized in nuclear industries.

### 2.3. Experimental condition & Calculation methodology

For model validation, CHF experimental data with annulus and tube geometry were used. All experiments used water as the working fluid. The validation range for the CFD calculation is summarized in Table II. Only DNB conditions were considered in selecting the test cases because the model set was chosen considering the bubbly flow region.

Table II. Experimental condition

Table II. Experimental condition				
Author	Thomson [5] (Tube)	Beus [6] (Annulus)	Janssen [7] (Annulus)	
Pressure (MPa)	13.79	13.79~15.5	6.7~9.7	
Mass flux (kg/m <sup>2</sup> s)	680~2,888	1,350~3,70 0	381~5,913	
Exit quality (-)	-0.19~ -0.18	-0.323~ -0.025	-0.04~ -0.016	
Equivalent diameter (mm)	4.75~11.1	5.6	4.6~12.7	
Heated length (mm)	318~1,828	2,134	1,518~3,051	

The computational meshes were generated using directed mesh and polygonal mesh option as shown in Figure 1. In the case of an annulus, only a quarter of the domain is simulated to save computational cost. Mesh convergence was verified by examining the axial wall temperature distribution. The high- $y^+$  wall function model was used, and the near-wall mesh was generated to maintain  $y^+>50$ . This selection is based on CASL reports [4].

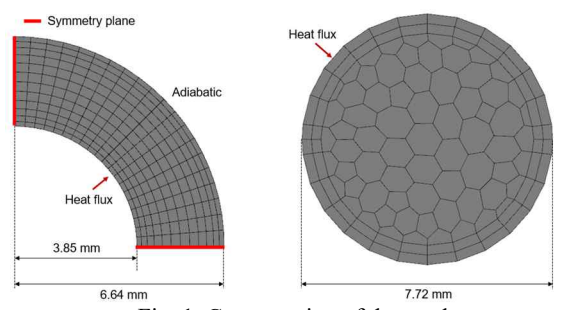


Fig. 1. Cross-section of the mesh

As shown in Figure 2, CHF was determined by gradually increasing the wall heat flux in steps until a rapid change in wall temperature was observed. The boiling curve derived from the simulation results confirmed that the heat flux at the onset of temperature excursion corresponds to the CHF point. Figure 3 illustrates an example of the boiling curve.

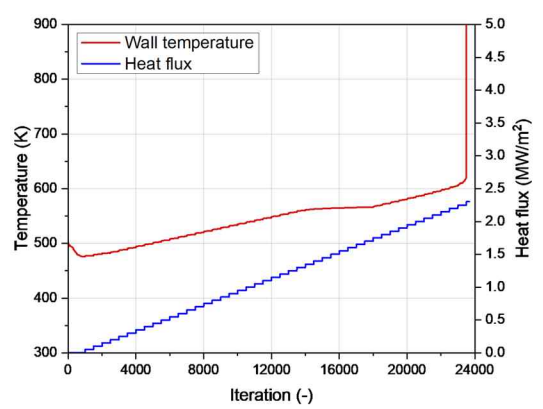


Fig. 2. CHF calculation method

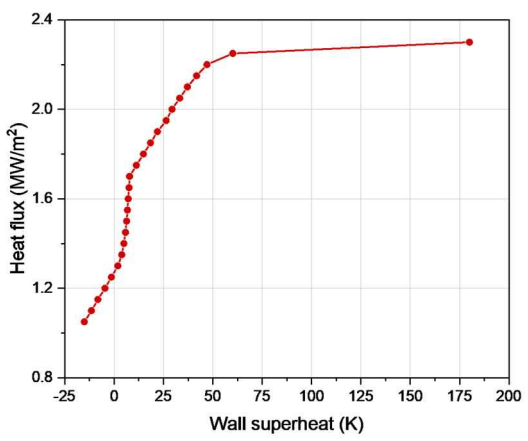


Fig. 3. Boiling curve

## 3. Calculation results

# 3.1. Validation of the present models

Figure 4 compares the CHF values predicted by the present model with experimental data for both tubes and the annulus. For the tube case, all data fall within a 20% error, demonstrating the good predictive capability of the model. In contrast, for the annulus case, the predictive performance varies depending on the experimental dataset. For the Janssen data, all results lie within 30% error, whereas for the Beus data, the model exhibits relatively low predictive performance.

# 3.2. Comparative Validation of the CASL FY19 and present models

As mentioned earlier, the CASL FY19 model has been validated for tube and fuel assembly geometries; however, its predictive performance for CHF in the annulus has not been verified. Therefore, in this section,

the CHF prediction capability of CASL FY19 in the annulus is compared to the present model. As shown in Figure 5, the CASL FY19 model exhibits a clear underestimation trend for the Janssen database.

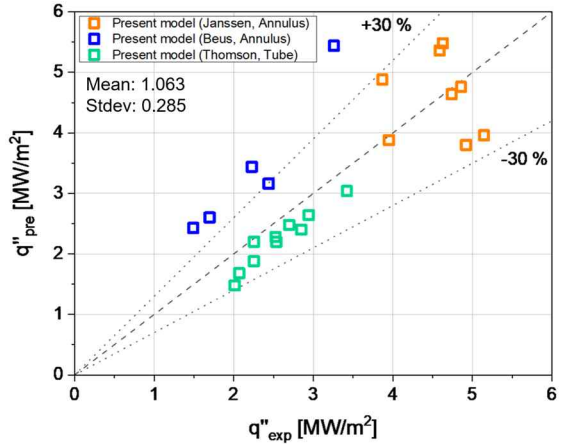


Fig. 4. Calculated CHF with present model for tube and annulus

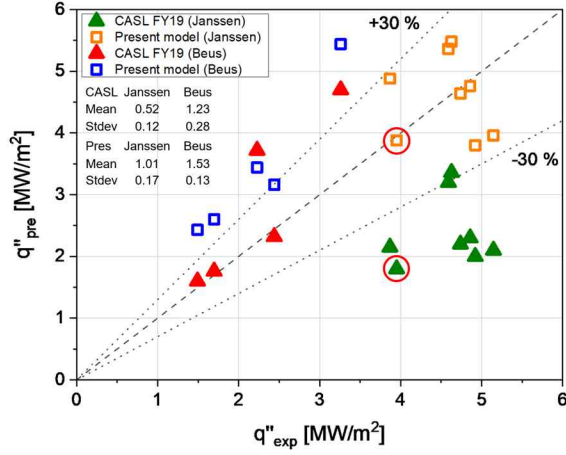


Fig. 5. Calculated CHF compared with experimental CHF for CASL FY19 and present model

To compare the differences in predictive performance evident in the Janssen data, radial void fraction distributions at the outlet were compared. As shown in Figure 6, the CASL FY19 model exhibited a void fraction of 1 at approximately half the experimental CHF value, resulting in CHF. Each case is indicated red circle in Figure 5.

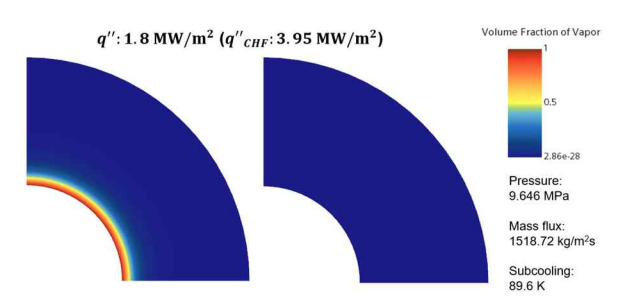


Fig. 6. Radial void fraction distribution (a) CASL FY19, and (b) present model

In contrast, the present model exhibited a void fraction

close to 0 throughout the entire region. Since the closure used to simulate wall boiling is the same for both models, this difference is likely due to differences in the applied momentum and condensation models. Therefore, it can be confirmed that the selection of appropriate momentum and condensation closure models exerts a significant influence on the accuracy of CFD-based CHF predictions.

For the Beus database, neither model exhibits strong predictive performance. The CASL FY19 model shows higher accuracy but lower precision, while the present model yields lower accuracy but higher precision.

#### 3.3. Error analysis

These variations in prediction accuracy highlight the system-condition dependence of the physical closures embedded in the solver. Therefore, error trends were examined concerning selected parameters to guide future model improvements.

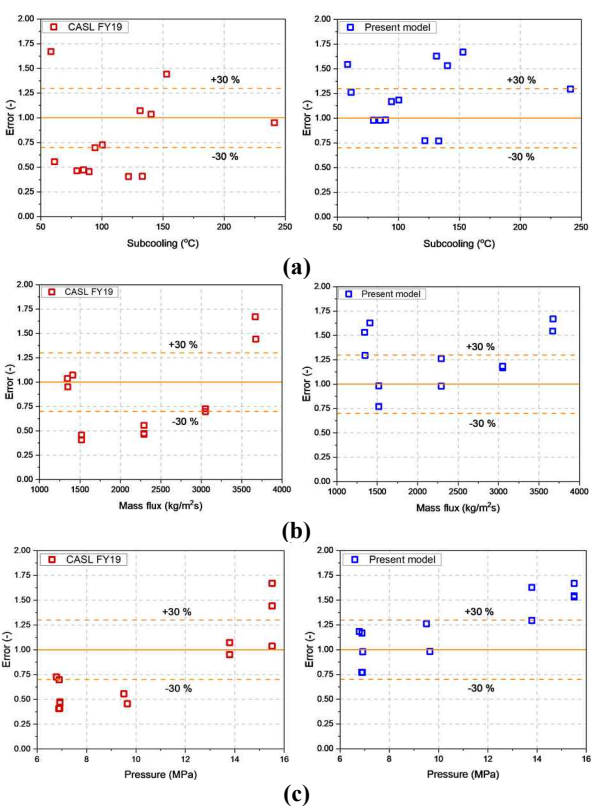


Fig. 7. Error categorized by (a) subcooling, (b) mass flux, and (c) pressure.

As shown in Figure 7, no clear trend was observed concerning inlet subcooling or mass flux. However, A clear system-pressure dependence is observed. The present model is more accurate at low pressures, while the CASL FY19 correlation underpredicts CHF. At high pressures, the present model overpredicts CHF, and the CASL FY19 model improves but remains insufficiently accurate.

#### 4. Conclusion

This study proposed the combination of the models for predicting DNB in tube and annulus geometries with CFD methodology. Especially, for annulus geometries, the predictive performance of the present model was compared with that of the CASL FY19 model developed as part of the CASL project.

The present model exhibits good predictive capability for the tube database. However, for the annulus case, errors exceeding 30% are observed for specific datasets. In addition, the CHF prediction performance of CASL FY19 was evaluated through comparison with the present model. For the Janssen database, the present model shows better predictive performance. For the Beus database, the present model exhibits lower accuracy than CASL FY19. However, it has higher precision.

A clear trend was observed with respect to system pressure; the CASL FY19 model exhibited relatively large errors at low pressures, whereas the present model demonstrated higher accuracy under low-pressure conditions but diminished accuracy at higher pressures. Further, assessment of CHF over a wide pressure range is planned for future investigation.

### ACKNOWLEDGMENT

This work was supported by the Nuclear Safety Research Program through the Korea Foundation Of Nuclear Safety (KoFONS) using the financial resource granted by the Nuclear Safety and Security Commission (NSSC) of the Republic of Korea (RS-2025-02311287)

#### REFERENCES

- [1] B. W. Yang, H. Anglart, B. Han, A. Liu Progress in rod bundle CHF in the past 40 years, Nuclear Engineering and Design, vol. 376, 2021.
- [2] S. J. Kim, R. C. J, J. S. Yoo, E. Baglietto, Progress Toward Simulating Departure from Nucleate Boiling at High-Pressure Applications with Selected Wall Boiling Closures, Nuclear Science and Engineering, Vol. 194, pp.690-707, 2020.
- [3] N. Kurul and M. Podowski, Multidimensional effects in forced convection subcooled boiling, in Proceedings Ninth International Heat Transfer Conference, 1990.
- [4] Weisman, J. and B. Pei, Prediction of critical heat flux in flow boiling at low qualities, International Journal of Heat and Mass Transfer, 26(10), 1463-1477, 1983.
- [5] Feng, J., (2019) Finalize CASL closure Models with Wall Model Improvements including Nucleation Site Density and Bubble Departure diameter CASL Report CASL Milestone L2:THM.DNB.P19.02
- [6] A. Tomiyama et al. Drag Coefficient of Single Bubble under Normal and Micro Gravity Conditions, JSME (1998).
- [7] Beus, S. G., & Seebold, O. P., Critical heat flux experiments in an internally heated annulus with a non-uniform, alternate high and low axial heat flux distribution (AWBA Development Program), (1981)
- [8] Janssen, E and Kervinen, J A., BURNOUT CONDITIONS FOR SINGLE ROD IN ANNULAR GEOMETRY, WATER AT 600 TO 1400 PSIA, Jan. 1963.